Thermodynamic Assessment of the Aluminum-Manganese (Al-Mn) Binary Phase Diagram

X.J. Liu, I. Ohnuma, R. Kainuma, and K. Ishida

(Submitted 8 December 1997; in revised form 3 August 1998)

A thermodynamic calculation of the Al-Mn binary system that takes into account recent experimental results and includes five intermetallic compounds and all the solid-solution phases is presented. The Gibbs energy of the body-centered cubic (bcc) phase has been described on the basis of the two-sublattice model that includes the second-order *A*2/*B*2 ordering reaction as well. A consistent set of optimized thermodynamic parameters has been arrived at for describing the Gibbs energy of each phase in this system leading to a better fit between calculation and experiments.

1. Introduction

A large number of experimental investigations have been directed toward the establishment of phase equilibria in the Al-Mn system because of its practical importance in the field of Al-base alloys and in the area of permanent magnet materials. The results of studies prior to 1987 were summarized by [90Mca] and are reproduced in Fig. 1, and the stable phases that appear in the Al-Mn system are listed in Table 1. More recently, the present authors have investigated the phase equilibria in the Mn-rich portion in detail by means of the diffusion couple technique and have modified some phase relations associated with the ε phase, as shown in Fig. 2 [96Liu].

Thermodynamic analyses of the Al-Mn system have been conducted previously by [78Kau], [87Mur], and [92Jan]. [92Jan] has critically assessed the Al-Mn system and has used the optimized thermodynamic parameters obtained to extend the assessment to higher-order systems such as the Al-Mn-Fe and Al-Mn-Fe-Si showing that reasonable agreement between calculation and experimental results could be obtained in the Al-rich portion of the ternary and quaternary diagrams [97Jan].

However, the assessment of the binary Al-Mn system by [92Jan] needs to be revised in the wake of recent experimental data determined by [96Liu]. The calculated phase equilibria in

X.J. Liu, I. Ohnuma, R. Kainuma, and **K. Ishida,** Department of Materials Science, Graduate School of Engineering, Tohoku University, Sendai 980-8579, Japan.

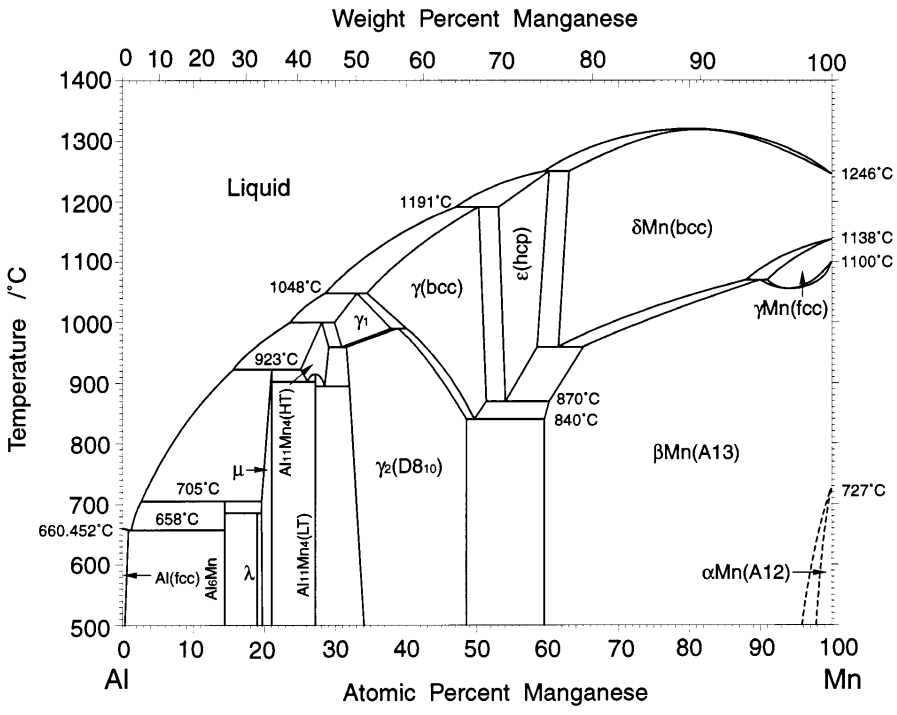

Fig. 1 The Al-Mn phase diagram compiled by [90Mca]

the Mn-rich portion of the Al-Mn diagrams are in serious disagreement with the experimental results. In addition, the γ phase present in the composition range 35 to 55 at.% Mn, which has been confirmed as a body-centered cubic (bcc) structure by [90Ell], has also not been taken into consideration in the assessment of [92Jan].

Because an accurate thermodynamic description of a binary system is crucial for the prediction of phase relations in ternary and higher-order systems, a reassessment of the Al-Mn system has been undertaken, and the results are reported.

2. An Overview of Previous Thermodynamic Assessments

The results of the first attempt at thermodynamic calculation of the whole system by [78Kau] yielded a diagram that differed considerably from the accepted Al-Mn phase diagram. Later, [87Mur] carried out a thermodynamic analysis of the liquid, face-centered cubic (fcc), and the stoichiometric phases in the Al-rich portion, with the limited aim of reproducing the phase equilibria in the Al-rich portion of the diagram.

Table 1 Stable phases in the Al-Mn system and the models used in the present assessment

Phase	Composition, at.% Mn	Strukturbericht designation	Prototype	Modeling phase	Model used in this study(a)
(Al)	0-0.62	*A*1	Cu	fcc	RSM
$Al_{12}Mn$	7.7	Unknown	Unknown	$Al_{12}Mn$	TSLM
Al_6Mn	14.2	$D2_h$	Al_6Mn	Al_6Mn	TSLM
λ	16.8-19	Unknown	Unknown	Al_4Mn	TSLM
μ	19-20.8	Unknown	Unknown	Al_4Mn	TSLM
$Al_{11}Mn_4$ (higher temperature)	27	Unknown	Unknown	$Al_{11}Mn_4$	TSLM
$Al_{11}Mn_4$ (lower temperature)	25-28.7	Unknown	Unknown	$Al_{11}Mn_4$	TSLM
γ_1	30-38.7	Unknown	Unknown	Al_8Mn_5	TSLM
γ_2	31.4-50	$D8_{10}$	Cr_5Al_8	Al_8Mn_5	TSLM
γ	34.5-52	*A*2	W	bcc	TSLM
ε	53.2-72	*A*3	Mg	cph	RSM
δMn	71-100	*A*2	W	bcc	TSLM
γMn	90.9-100	*A*1	Cu	fcc	RSM
βMn	59.5-100	*A*13	βMn	βMn	RSM
αMn	98-100	*A*12	αMn	αMn	RSM

(a) RSM, regular solution model; TSLM, two-sublattice model

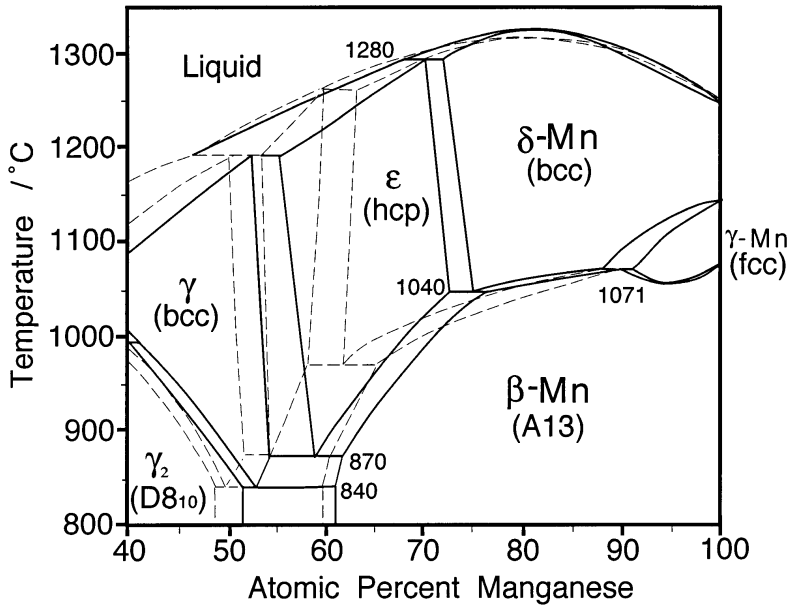

Fig. 2 Mn-rich portion of the Al-Mn binary phase diagram determined by [96Liu] with a comparison with that compiled by [90Mca]. Solid line, [96Liu]; dashed line, [90Mca]

A complete assessment of the Al-Mn binary phase diagram over the whole composition range, which took into account the thermodynamic data and phase equilibria information from [72Bat], [73Esi], and [60Kub], was published by [92Jan], as shown in Fig. 3. Although his calculated results are in basic agreement with the diagram compiled by [90Mca], as compared in Fig. 2 and 3, it is obvious that there is a significant difference between the two in the composition range above 40 at.% Mn. The following are the main differences between the experimental results and the calculated diagram of [92Jan]:

- The ε/δMn phase equilibrium established by [60Kos] was not well reproduced in the calculation [92Jan] due to the lack of reliable experimental information. The recent experimental data of [96Liu] have confirmed that the stability range of the ε phase is larger than that predicted by calculation.
- The phase equilibria among γ, γ_1, and γ_2 phases in the 30 to ~50 at.% Mn composition range were determined by [71God], but the crystal structures of these phases were not determined. In the assessment of [92Jan], all the γ, γ_1, and γ_2 phases were assigned the same γ_2 single phase with $D8_{10}$ structure [69Sch], thus precluding the possibility of separate phase equilibria between these three phases. As a consequence of ignoring the γ/γ_2 phase equilibrium, the presence of the eutectoid reaction $\gamma(\text{bcc}) \leftrightarrow \gamma_2$ ($D8_{10}$:Al_8Mn_5) + βMn(*A*13) was also not considered, even though the existence of this invariant reaction had been confirmed by [58Kon], [60Koc], and [60Kos].
- [90Ell] had reported that the γ phase had the bcc structure using high-temperature XRD. It has also been noted in the recent reviews by [94Oka1], [94Oka2], and [97Oka] that the γ and δMn phases in the Al-Mn system have the same bcc structure, and, therefore, the phase boundaries between δMn/liquid and γ/liquid phase equilibria should be a smooth continuous curve throughout the ε/liquid phase equilibrium composition range.

3. Evaluation and Selection of Experimental Information

3.1 Experimental Information Prior to 1987

Data pertaining to investigations on the phase equilibria and thermodynamic properties were first summarized by [90Mca] and assessed by [92Jan]. In the present assessment, the heats of formation of the compounds Al_6Mn, Al_4Mn, $Al_{11}Mn_4$, and Al_8Mn_5 from earlier published data have been utilized. Regarding the compound γ_2 (Al_8Mn_5), the literature value is used only as a reference, as it is felt that the measurement error in the reported values might be large because (a) two different values were given in the original paper, and (b) the alloy (50 at.% Mn) used in the experiment might have fallen in the γ_2 + βMn two-phase region. The data from [58Kon], [60Koc], [60Kos], and [71God] have been used to assess the liquidus, solidus, and the other phase equilibria in the composition range below 50 at.% Mn.

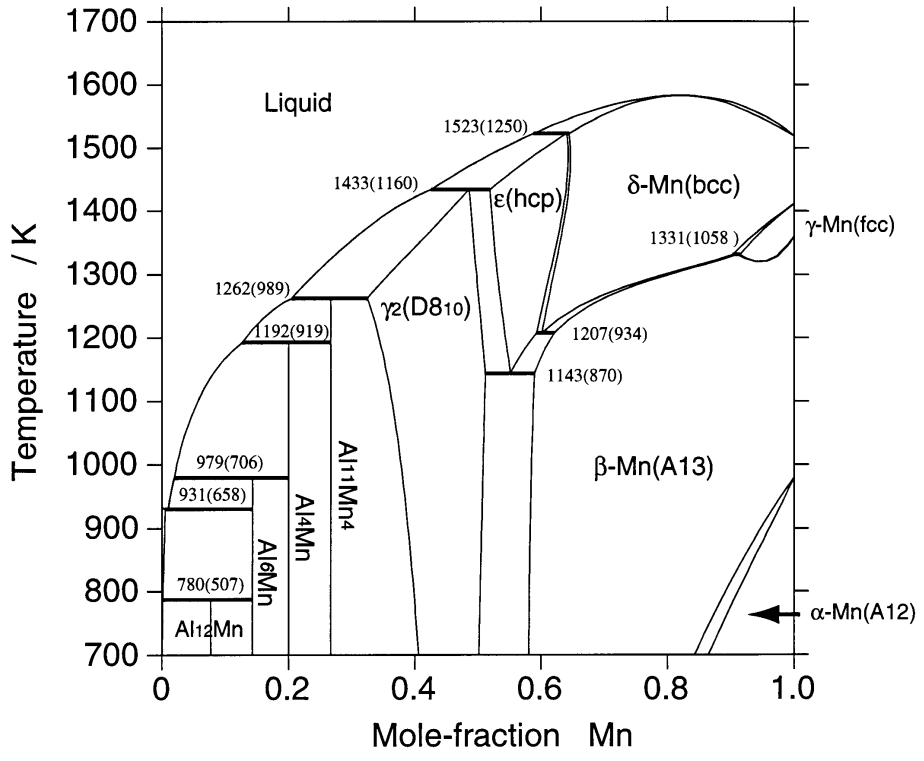

Fig. 3 The Al-Mn phase diagram calculated by [92Jan]. The numbers in brackets indicate the temperature in °C.

3.2 Ordering in the γ Phase

Although [90Ell] had confirmed that γ phase had a bcc structure, he had not reported the occurrence of an *A*2/*B*2 order-disorder transformation. However, because the enthalpy of mixing between Mn and Al in the liquid phase shows a large negative value [83Nis], it is quite reasonable to expect that the Al and Mn atoms in solid γ phase would have a tendency to order. This expectation is further strengthened by the experimental results and the preliminary calculations of the ordering reactions in the Co-Al-Cr, Co-Al-Mn, Ni-Al-Mn, and Cu-Al-Mn ternary systems [98Ish], [98Kai1], [98Kai2], and [98Liu]. In addition, preliminary results from differential scanning calorimetry (DSC) traces obtained on two Al-Mn alloys with 49 at.% Al and 52 at.% Al, respectively, indicate that the 49 at.% Al alloy has a peak at 1238 K and the 52 at.% Al alloy a peak at 1240 K [98Liu]. The occurrence of these peaks has been taken as sufficient evidence for an ordering reaction, and the temperatures associated with them have been taken as the *A*2/*B*2 ordering temperatures of γ phase in the present assessment for calculating the phase diagram, although further experiments are needed to confirm this result.

3.3 Phase Equilibria Associated with the ε Phase

The data of [96Liu] have been used extensively in the present assessment of the phase equilibria in the Mn-rich portion. [96Liu] reported that the ε/δMn phase boundary was located at approximately 72 at.% Mn and that the ε phase extended to higher Mn content than that reported before. This departure from previous results was attributed to the presence of previously undetected transformation of ε to βMn that occurs on quenching. It was also determined that the eutectoid reaction δMn(fcc) ↔ ε(cph) + βMn occurred at approximately 1040 °C, which is higher than 970 °C reported in earlier papers. These new findings in the binary Al-Mn system seem to be consistent with the results from some ternary systems such as Co-Al-Mn and Ni-Al-Mn [98Kai1].

The examination of experimental results on the ε/δMn phase equilibrium reported by previous authors reveals that they were derived from thermal analysis and hardness measurements [60Kos]. The reliability of such methods is questionable, particularly in the context of the ε/δMn equilibrium in the Al-Mn system, for the following reasons:

- Thermal analysis is not a suitable method for determining the γ/ε and ε/δMn phase equilibria in the Al-Mn system because the phase boundaries are very steep and almost parallel to the temperature axis.
- Microhardness measurements have to be treated carefully because information from microhardness measurements could sometimes be wrongly interpreted, especially when a phase transformation occurs on quenching. [96Liu] had detected a hardness gap in the diffusion couple at a composition of about 56 at.% Mn in agreement with the data of [60Kos]. However, in light of the fact that no composition gap had occurred and the continuity of the concentration profile was still retained at this composition, the hardness gap could only be attributed to a phase transformation that had occurred on quenching.

Another recent study, with a special interest in the stability of τ phase, has been carried out by [96Mul] in the composition range 50 to 65 at.% Mn using DTA. Five invariant reactions γ ↔ γ_2 + βMn, ε ↔ γ + βMn, γMn ↔ ε + βMn, liquid + δMn ↔ ε, and liquid + ε ↔ γ are reported. The temperatures and compositions corresponding to the two peritectic reactions liquid + δMn ↔ ε and liquid + ε ↔ γ are in agreement with the ones reported earlier [71God]. However, some discrepancies still exist, which are as follows:

- The temperatures corresponding to the eutectoid reactions γ ↔ γ_2 + βMn and ε ↔ γ + βMn are located at about 1090 and 1130 K, which are about 10 and 15 K lower, respectively, than those reported by [58Kon], [60Koc], and [71God].
- The temperature of the eutectoid reaction δMn(bcc) ↔ ε + βMn has been determined as 1176 K, which is lower than that reported by [96Liu].

These data from [96Mul] have not been included in the assessment for the following reasons. In their investigation, DTA has been the only experimental method employed to determine the phase equilibria. Moreover, as no experimental data on the ε/γ and ε/δMn phase equilibria have been included by them in their original paper, it is quite likely that they have not determined the ε/δMn phase equilibrium. This could have given rise to a large error in determination of the δMn ↔ ε + βMn eutectoid reaction temperature.

4. Gibbs Energy Models

4.1 Liquid, γMn, ε, βMn, and αMn(A12) Phases

The regular solution model has been employed to describe the Gibbs free energies of liquid, γMn, ε, βMn, and αMn phases.

4.2 bcc Phases (δMn and γ Phases)

In order to describe the ordering in the γ phase (bcc), the Gibbs energy of the bcc phase has been described on the basis of the two-sublattice model proposed by [70Hil], which is expressed as follows:

$$\begin{aligned} G_m = {} & y^{I}_{Al}\, y^{II}_{Al}\, {}^0G_{AlAl} + y^{I}_{Al}\, y^{II}_{Mn}\, {}^0G_{AlMn} + y^{I}_{Mn}\, y^{II}_{Al}\, {}^0G_{MnAl} \\ & + y^{I}_{Mn}\, y^{II}_{Mn}\, {}^0G_{MnMn} + 0.5\,RT \sum_{\substack{s=I,II \\ i=Al,Mn}} y^{s}_{i} \ln y^{s}_{i} \\ & + L^{Al}_{AlMn}\,(y^{I}_{Al}\, y^{I}_{Mn}\, y^{II}_{Al} + y^{I}_{Al}\, y^{II}_{Al}\, y^{II}_{Mn}) \\ & + L^{Mn}_{AlMn}\,(y^{I}_{Mn}\, y^{II}_{Al}\, y^{II}_{Mn} + y^{I}_{Mn}\, y^{I}_{Al}\, y^{II}_{Mn}) \end{aligned} \qquad \text{(Eq 1)}$$

where y^{s}_{i} represents the site fraction of constituent *i* in the sublattice *s*. The four ${}^0G$ terms represent the Gibbs energy of formation of the compounds constituting the solution, these compounds being real or hypothetical. The interaction coefficients can vary with temperature and composition.

4.3 Compound Phases

The modeling of the compound phases is based on the treatment of [92Jan]. The γ_2 (Al_8Mn_5) phase has been simplified to

include only three sublattices. The Gibbs energy per atom mole is given by:

$$G^{\gamma_2} = y_{Al}\,{}^0G_{Al:Mn:Al} + y_{Mn}\,{}^0G_{Al:Mn:Mn} + \frac{5}{13}\,RT\,(y_{Al}\ln y_{Al} + y_{Al}\ln y_{Al}) + y_{Al}\,y_{Mn}\sum_{n=0}^{2} {}^nL_{Al,Mn}(y_{Al}-y_{Mn})^n \qquad \text{(Eq 2)}$$

where y denotes the site fraction on the third sublattice, and ${}^nL_{Al,Mn}$ the temperature-dependent term.

The Gibbs energies of formation of the stoichiometric phases $Al_{12}Mn$, Al_6Mn, Al_4Mn, and $Al_{11}Mn_4$ are based on a two-sublattice model, which is written as follows:

$$\Delta G_{Al_pMn_q} = {}^0G^{Al_pMn_q} - p\,{}^0G^{fcc}_{Al} - q\,{}^0G^{\alpha Mn}_{Mn} \qquad \text{(Eq 3)}$$

where ${}^0G^{Al_pMn_q}$ expresses the Gibbs energy of the compound phase Al_pMn_q.

The lattice stabilities of pure elements Al and Mn have been taken from [91Din] and [90Fer], respectively. The magnetic contribution to the Gibbs energy for some phases has also been considered and described by a phenomenological model originally presented by [76Ind] and modified by [78Hil]. In the present assessment the Néel temperature (T_N) has been taken as the critical magnetic transition temperature for Mn, while it has been set at zero for Al in the same phases. The magnetic parameters used in this calculation are summarized in Table 2. However, magnetic contributions to free energies in this system are negligible because the T_N is rather low.

5. Computerized Optimization

5.1 Optimization

The evaluation of thermodynamic parameters has been made using the computer software PARROT developed by [85Sun]. The liquid phase parameters as assessed by [92Jan] are found to be acceptable for an adequate description of the liquid phase and have been used in the present work with no alterations.

Optimization was initiated by first fixing the parameters of the liquid phase. This was followed by the evaluation of the parameters for the different phases in the following sequence: the bcc, cph, βMn, γMn, αMn, $\gamma_2(Al_8Mn_5)$ phases, and lastly the compounds in the Al-rich portion.

The difficulty encountered in assigning the correct parameters to the ε phase, which is surrounded by the bcc phase, using only the data pertaining to the δMn/ε, ε/γ, and liquid/ε phase equilibria, was overcome by introducing a second-order Redlich-Kister parameter in the Gibbs energy expression and obtaining the best fit between calculation and experiment. Another difficulty that arose during the optimization of the parameters for the γ_2 phase was the matching of the calculated and experimental γ/γ_2 phase equilibrium. This was achieved by optimizing the energy of formation and interaction parameters of the γ_2 phase.

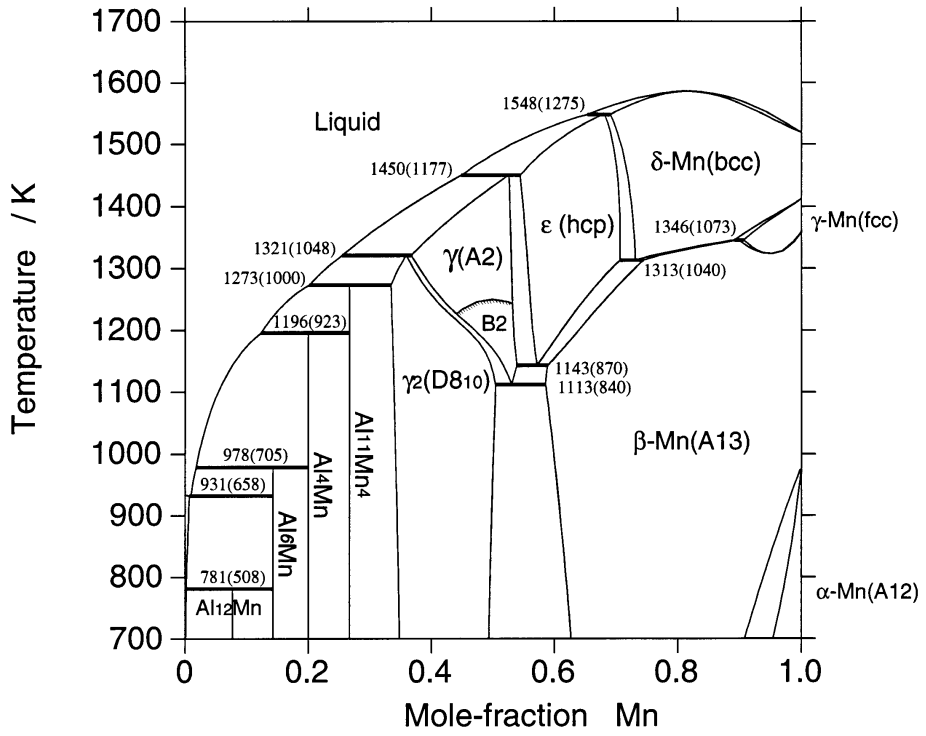

Fig. 4 The reassessed phase diagram of the Al-Mn system according to the present assessment. The numbers in brackets indicate the temperature in °C.

Table 2 Summary of the thermodynamic parameters used in the calculation of the phase diagram in the Al-Mn binary system

Liquid; constituent Mn, Al

For 298.1-933.59 K:

$${}^0G^{L}_{Al} - {}^0G^{fcc}_{Al} = 11{,}005.6 - 11.8409\ T + 7.9043 \times 10^{-20}\ T^7$$

For 933.59-2900.00 K:

$${}^0G^{L}_{Al} - {}^0G^{fcc}_{Al} = 10{,}482.6 - 11.252\ T + 1.23426 \times 10^{28}\ T^{-9}$$

For 298.15-1519.00 K:

$${}^0G^{L}_{Mn} - H^{SER}_{Mn} = 9744.63 + 117.4382\ T - 23.4582\ T \ln T - 0.00734768\ T^2 + 69{,}827.1\ T^{-1} - 4.419297 \times 10^{21}\ T^7$$

For 1519.00-6000.00 K:

$${}^0G^{L}_{Mn} - H^{SER}_{Mn} = -9993.9 + 299.036\ T - 48\ T \ln T$$

$${}^0L^{L}_{Al,Mn} = -66{,}174 + 27.0988\ T$$

$${}^1L^{L}_{Al,Mn} = -7509 + 5.4836\ T$$

$${}^2L^{L}_{Al,Mn} = -2639$$

$Al_{12}Mn$: two sublattices, sites 0.923077: 0.076923; constituents Al:Mn

$${}^0G^{Al_{12}Mn} - 0.923077\ {}^0G^{fcc}_{Al} - 0.076923\ {}^0G^{\alpha Mn}_{Al} = -8174.2312 + 2.583446\ T$$

Al_6Mn; two sublattices, sites 0.857143: 0.142857; constituent Al:Mn

$${}^0G^{Al_6Mn} - 0.857143\ {}^0G^{fcc}_{Al} - 0.142857\ {}^0G^{\alpha Mn}_{Al} = -15{,}064.2857 + 4.665614\ T$$

Al_4Mn; two sublattices, sites 0.8: 0.2; constituents Al:Mn

$${}^0G^{Al_4Mn} - 0.8\ {}^0G^{fcc}_{Al} - 0.2\ {}^0G^{\alpha Mn}_{Al} = -21{,}230 + 6.9522\ T$$

$Al_{11}Mn_4$; two sublattices, sites 0.7333, 0.2667; constituents Al:Mn

$${}^0G^{Al_{11}Mn_4} - 0.7333\ {}^0G^{fcc}_{Al} - 0.2667\ {}^0G^{\alpha Mn}_{Al} = -22{,}746.245 + 6.0\ T$$

αMn (*A*12); constituents Al,Mn

$${}^0G^{\alpha}_{Al} - {}^0G^{fcc}_{Al} = 10{,}083.4 - 4.813\ T$$

For 298.15-1519.00 K:

$${}^0G^{\alpha}_{Mn} - H^{SER}_{Mn} = -8115.28 + 130.059\ T - 23.4582\ T \ln T - 0.00734768\ T^2 + 69{,}827.1\ T^{-1}$$

For 1519.0-3000.00 K:

$${}^0G^{\alpha}_{Mn} - H^{SER}_{Mn} = -28{,}733.41 + 312.2648\ T - 48\ T \ln T + 1.656847 \times 10^{30}\ T^{-9}$$

$${}^0L^{\alpha}_{Al,Mn} = -105{,}000 + 56.5\ T$$

fcc (γMn phase); consitutents Al,Mn

For 298.15-700.00 K:

$${}^0G^{fcc}_{Al} - H^{SER}_{Al} = -7976.15 + 137.072\ T - 24.3672\ T \ln T - 0.00188466\ T^2 - 8.77664 \times 10^{-7}\ T^3 + 74{,}092.4\ T^{-1}$$

For 700.00-933.59 K:

$${}^0G^{fcc}_{Al} - H^{SER}_{Al} = -11{,}267.2 + 233.02\ T - 38.5844\ T \ln T - 0.018532\ T^2 - 5.76423 \times 10^{-6}\ T^3 + 74{,}092.4\ T^{-1}$$

For 933.59-2900.00 K:

$${}^0G^{fcc}_{Al} - H^{SER}_{Al} = -11{,}277.7 + 188.662\ T - 31.7482\ T \ln T - 1.23426 \times 10^{28}\ T^{-9}$$

For 298.15-1519.00 K:

$${}^0G^{fcc}_{Mn} - H^{SER}_{Mn} = -3439.3 + 131.884\ T - 24.5177\ T \ln T - 0.006\ T^2 + 69{,}600\ T^{-1}$$

For 1519.0-6000.00 K:

$${}^0G^{fcc}_{Mn} - H^{SER}_{Mn} = -26{,}070 + 309.6664\ T - 48\ T \ln T + 3.8619645 \times 10^{30}\ T^{-9}$$

$${}^0L^{fcc}_{Al,Mn} = -83{,}829 + 37.6788\ T$$

$${}^1L^{fcc}_{Al,Mn} = 18{,}378 - 5.07T$$

cph (ε phase); consitituents Al,Mn

$${}^0G^{cph}_{Al} - {}^0G^{fcc}_{Al} = 5481 - 1.8\ T$$

For 298.15-1519.00 K:

$${}^0G^{cph}_{Mn} - H^{SER}_{Mn} = -4440.3 + 133.007\ T - 24.5177\ T \ln T - 0.006\ T^2 + 69{,}600\ T^{-1}$$

For 1519.0-6000.00 K:

$${}^0G^{cph}_{Mn} - H^{SER}_{Mn} = -27{,}071.1 + 310.7894\ T - 48\ T \ln T + 3.8619645 \times 10^{30}\ T^{-9}$$

$${}^0L^{cph}_{Al,Mn} = -102{,}387.99 + 40.02576\ T$$

All values in SI units per one mole of atoms for each phase. Magnetic parameters are also given.

(continued)

Table 2 Summary of the thermodynamic parameters used in the calculation of the phase diagram in the Al-Mn binary system (continued)

cph (ε phase); consitituents Al,Mn (continued)

$^{1}L^{cph}_{Al,Mn} = -9204.014 + 11.726\ T$

$^{2}L^{cph}_{Al,Mn} = 132{,}282.06 - 82.097\ T$

bcc (γ and δMn phases); two sublattices 0.5:0.5; consitituents Al,Mn:Al,Mn

$^{0}G^{bcc}_{Al} - {}^{0}G^{fcc}_{Al} = 10{,}083 - 4.813\ T$

For 298.15-1519.00 K:

$^{0}G^{bcc}_{Mn} - H^{SER}_{Mn} = -3235.3 + 127.85\ T - 23.7\ T \ln T - 0.00744271\ T^{2} + 60.0\ T^{-1}$

For 1519-6000.00 K:

$^{0}G^{bcc}_{Mn} - H^{SER}_{Mn} = -23{,}188.83 + 307.7043\ T - 48\ T \ln T + 1.265152 \times 10^{30}\ T^{-9}$

$^{0}G^{bcc}_{Al:Mn} = 0.5\ {}^{0}G^{bcc}_{Al} + 0.5\ {}^{0}G^{bcc}_{Mn} - 34{,}676.32 + 12.622\ T$

$^{0}L^{Al}_{Al:Mn} = -29{,}739.82 + 34.5888\ T$

$^{1}L^{Al}_{Al:Mn} = -984.5 + 6.6555\ T$

$^{0}L^{Mn}_{Al:Mn} = -23{,}832.82 - 5.3448\ T$

$^{1}L^{Mn}_{Al:Mn} = -984.5 + 6.6555\ T$

Al_8Mn_5; three sublattices, sites 0.4615, 0.1539, 0.3846; constituents Al: Mn: Al,Mn

$^{0}G^{Al_8Mn_5} - 0.8461\ {}^{0}G^{fcc}_{Al} - 0.1539\ {}^{0}G^{\alpha Mn}_{Al} = -12{,}427.462 + 5.6923\ T$

$^{0}G^{Al_8Mn_5} - 0.4615\ {}^{0}G^{fcc}_{Al} - 0.5385\ {}^{0}G^{\alpha Mn}_{Al} = -23{,}566.115 + 4.269\ T$

$^{0}L_{Al,Mn} = -30{,}265.677 + 15T$

$^{1}L_{Al,Mn} = 8977.966 - 12.7596\ T$

βMn(*A*13); constituents Al,Mn

$^{0}G^{\beta}_{Al} - {}^{0}G^{fcc}_{Al} = 10{,}920.44 - 4.8116\ T$

For 298.15-1519.00 K:

$^{0}G^{\beta}_{Mn} - G^{SER}_{Mn} = -5800.4 + 135.995\ T - 24.8785\ T \ln T - 0.00583359\,T^{2} + 70{,}269.1\ T^{-1}$

For 1519.0-6000.00 K:

$^{0}G^{\beta}_{Mn} - G^{SER}_{Mn} = -28{,}290.76 + 311.2933\ T - 48\ T \ln T + 3.9675699 \times 10^{30}\ T^{-9}$

$^{0}L^{\beta}_{Al,Mn} = -117{,}970.76 + 51.35\ T$

$^{1}L^{\beta}_{Al,Mn} = -6288.96$

Magnetism parameters

For the phases bcc, fcc, cph, and αMn, a magnetic contribution was added to the Gibbs energy functions listed above. The antiferromagnetic factors are –1 for bcc and –3 for fcc, cph, and αMn, respectively. The magnetic contribution to Gibbs energy is for the phase ϕ:

$^{mg}G^{\phi}_{m} = \mathrm{RT} \ln (\beta^{\phi} - 1)\ f(\tau)$

where $\tau = T/T^{\phi}_{N}$ and

for $\tau > 1 \quad f(\tau) = -\frac{1}{K}\left(\frac{\tau^{-5}}{10} + \frac{\tau^{-15}}{315} + \frac{\tau^{-25}}{1500}\right)$

for $\tau < 1 \quad f(\tau) = -\frac{1}{K}\left(-K + \frac{79}{140p\tau} + \frac{158}{497}\left(\frac{1}{p} - 1\right)\left(\frac{\tau^{3}}{2} + \frac{\tau^{9}}{45} + \frac{\tau^{15}}{200}\right)\right)$

where $K = \frac{518}{1125}\left(1 + \frac{790}{497}\left(\frac{1}{p} - 1\right)\right)$ and

$p = 0.40$ for bcc and 0.28 for fcc, cph, αMn phases.

Magnetic parameters were listed as follows:

$T^{bcc}_{N} = 580 X_{Mn}$

$\beta^{bcc} = 0.27 X_{Mn}$

$T^{fcc}_{N} = 540 X_{Mn}$

$\beta^{fcc} = 0.62 X_{Mn}$

$T^{cph}_{N} = 540 X_{Mn}$

$\beta^{cph} = 0.62 X_{Mn}$

$T^{\alpha Mn}_{N} = 95 X_{Mn}$

$\beta^{\alpha Mn} = 0.22 X_{Mn}$

All values in SI units per one mole of atoms for each phase. Magnetic parameters are also given.

Table 3 Comparison between the experimental and calculated invariant reactions in the Al-Mn phase diagram

Reaction	Reaction type	Temperature K	Temperature °C	Composition, at.% Mn			Reference
(Al) + $Al_6Mn \rightarrow Al_{12}Mn$	Peritectoid	781.0	508	0.23	7.69	14.29	This study
		780.3	507.3	0.21	7.69	14.29	[92Jan](a)
		777-793	504-520				[86Sch](b)
$L \rightarrow$ (Al) + Al_6Mn	Eutectic	931.5	658.5	0.96	0.71	14.29	This study
		931	658	1.00	0.71	14.29	[92Jan](a)
		931	658	1.00	0.62	14.2	[90Mca](c)
		931	658	0.99			[60Kos](b)
L + $Al_4Mn \rightarrow Al_6Mn$	Peritectic	978.2	705.2	1.82	20.00	14.29	This study
		979	706	1.94	20.00	14.29	[92Jan](a)
		978	705	2.40	19.0	14.2	[90Mca](c)
		978	705		19		[71God](b)
L + $Al_{11}Mn_4 \rightarrow Al_4Mn$	Peritectic	1196	923	12.33	26.67	20.00	This study
		1193	920	12.70	26.67	20.00	[92Jan](a)
		1196	923	15.2	25	20.8	[90Mca](c)
		1196	923	15	24.2	21	[71God](b)
L + $\gamma_2 \rightarrow Al_{11}Mn_4$	Peritectic	1273	1000	20.09	33.36	26.67	This study
		1263	990	20.49	32.48	26.67	[92Jan](a)
		1275	1002	23.2	30	28.63	[90Mca](c)
		1275	1002	22.3	30	28	[71God](b)
L + $\delta Mn \rightarrow \varepsilon$	Peritectic	1548	1275	65.38	69.02	68.09	This study
		1523	1250	58.98	64.54	64.22	[92Jan](a)
		1533	1260	59	60	63	[90Mca](c)
		1533	1260				[71God](b)
		1533	1280				[96Liu](b)
		1529	1256				[96Mul](b)
$\varepsilon \rightarrow \gamma + \beta Mn$	Eutectoid	1143	870	57.16	53.91	58.89	This study
		1143(d)	870	55.15	51.17	58.96	[92Jan](a)
		1143	870	54	51.3	60	[90Mca](c)
		1143	870				[71God](b)
		1143	870	55	50.5	60	[58Kon](b)
		1143	870	58	53.5	60.6	[96Liu](b)
		1130	857				[96Mul](b)
L + $\gamma \rightarrow \gamma_2$	Peritectic	1321	1048	25.52	36.74	35.93	This study
		1321	1048	28.3	34.5	33.6	[90Mca](c)
		1321	1048	28.3	34.5	33.6	[71God](b)
L + $\varepsilon \rightarrow \gamma$	Peritectic	1450	1177	44.90	54.44	52.64	This study
		1433	1160	42.54	51.86	48.58	[92Jan](a)
		1464	1191	43	53.2	50.6	[90Mca](c)
		1433	1160				[60Kos](b)
		1463	1190				[96Mul](b)
$\gamma \rightarrow \gamma_2 + \beta Mn$	Eutectoid	1113	840	53.10	50.01	58.21	This study
		1113	840	49.5	47	59.50	[71God](b)
		1113	840				[90Mca](c)
		1113	840	52.5	50.5	60	[60Koc](b)
		1090	817				[96Mul](b)
$\delta Mn + \gamma Mn \rightarrow \beta Mn$	Peritectoid	1346	1073	89.18	90.67	89.81	This study
		1331	1058	90.29	91.30	90.97	[92Jan](a)
		1344	1071	87.9	90.9	90	[90Mca](c)
$\delta Mn \rightarrow \varepsilon + \beta Mn$	Eutectoid	1313	1040	73.14	70.64	74.49	This study
		1208	935	60.19	59.32	62.17	[92Jan](a)
		1243	970	61.5	58	65	[90Mca](c)

(continued)

(a) Thermodynamic calculation. (b) Experimental data. (c) Assessment. (d) The temperature of the invariant reaction corresponds to the reaction $\varepsilon \rightarrow \gamma_2 + \beta Mn$ rather than $\varepsilon \rightarrow \gamma + \beta Mn$.

Table 3 Comparison between the experimental and calculated invariant reactions in the Al-Mn phase diagram (continued)

Reaction	Reaction type	Temperature K	Temperature °C	Composition, at.% Mn			Reference
δMn → ε + βMn (cont.)	Eutectoid (cont.)	1313	1040	74.5	71.5	75.5	[96Liu](b)
		1176	903				[96Mul](b)
L → δMn	Congruent point	1585	1312	81.70	81.70		This study
		1583	1310	81.98	81.98		[92Jan](a)
		1588	1315	80.3	80.3		[90Mca](c)
δMn → γMn	Congruent point	1323	1050	95.05	95.05		This study
		1327	1054	94.25	94.25		[92Jan](a)
		1328	1055	94	94		[90Mca](c)

(a) Thermodynamic calculation. (b) Experimental data. (c) Assessment. (d) The temperature of the invariant reaction corresponds to the reaction ε → γ_2 + βMn rather than ε → γ + βMn.

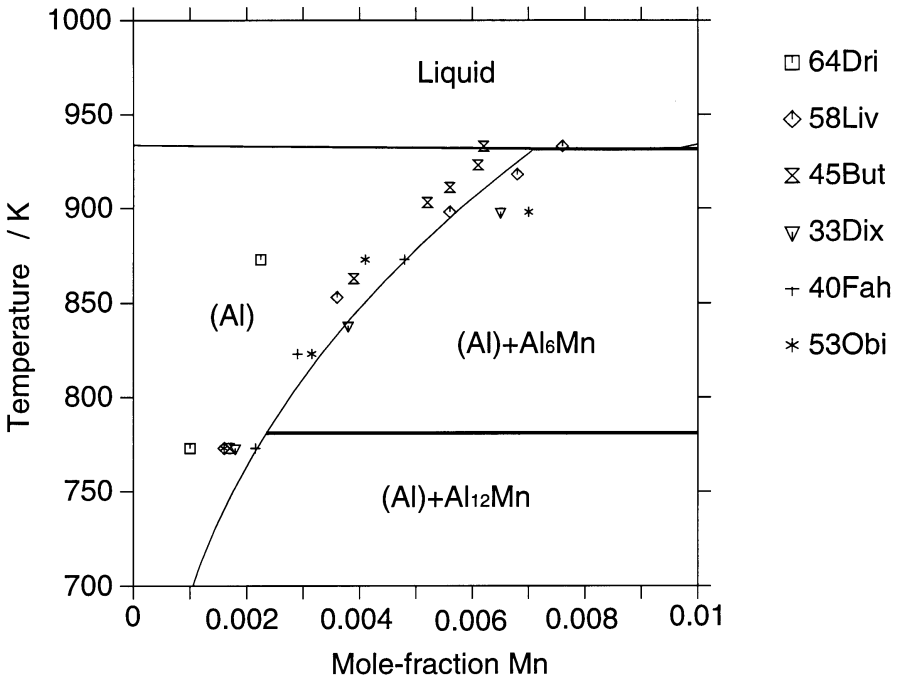

Fig. 5 Comparison of the calculated Mn solubility in fcc-Al with experimental data

5.2 Comparison and Discussion

The calculated Al-Mn phase diagram is shown in Fig. 4, and all the parameters describing each phase are listed in Table 2. Experimental and calculated results for all invariant reactions given in Table 3 show that there is very good agreement between experimental and calculated phase diagram characteristics. Calculated and experimental enthalpy values of the compounds are given in Table 4, along with the assessed values taken from [92Jan].

On referring to Fig. 3 and 4 one can see that the two calculated stability ranges for the $\gamma_2(Al_8Mn_5)$ phase, one by [92Jan] and the other by the present authors, differ quite significantly. According to the present work, the stable range for the γ_2 phase is wider than that calculated by [92Jan], but is much closer to the experimental phase diagram assessed by [90Mca].

The calculated phase diagram superimposed with experimental data points are split into three sections and shown in Fig. 5 to 7. Figure 5 is the phase diagram in the Al-rich composition region between 0 and 10 at.% Mn, Fig. 6 between 0 and 40 at.% Mn, and Fig. 7 between 30 and 100 at.% Mn. Figure 5 shows the calculated Mn solubility line in the fcc phase superimposed with experimental data from [33Dix], [40Fah], [43Phi], [45But], [53Obi], [58Liv], and [64Dri]. It is seen that the calculated values are in good agreement with experimental data. Figure 6 shows that while the calculated and experimental invariant reaction temperatures agree very well [33Dix], [43Phi], [71God], and [87Mur], the calculated

liquidus temperatures are slightly higher than the experimental values in the 10 to 20 at.% Mn region.

The calculated diagram superimposed with experimental results covering the region 30 to 100 at.% Mn, shown in Fig. 7, indicates that the calculated and experimental $\varepsilon \leftrightarrow \gamma + \beta Mn$ eutectoid reaction temperatures are in good agreement; it also shows that the results of [96Mul] are in better agreement with the calculated ones except for the temperatures of the eutectoid reactions $\varepsilon \leftrightarrow \gamma + \beta Mn$ and $\varepsilon \leftrightarrow \gamma + \beta Mn$. It is possible that the data at about 62 at.% Mn correspond to the $\varepsilon/\beta Mn$ phase

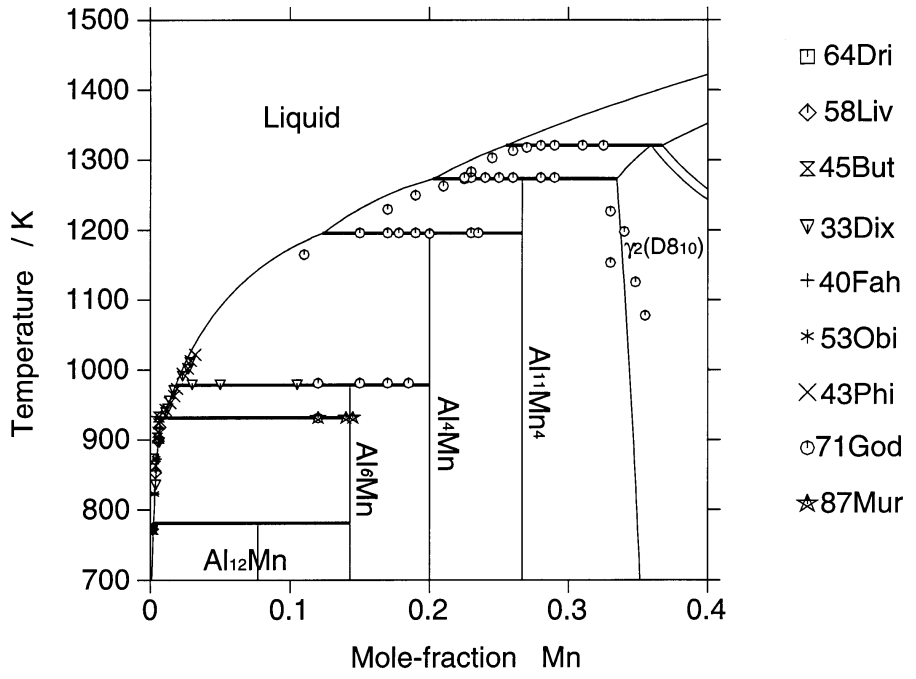

Fig. 6 Comparison of the calculated Al-rich part of the Al-Mn phase diagram with experimental data

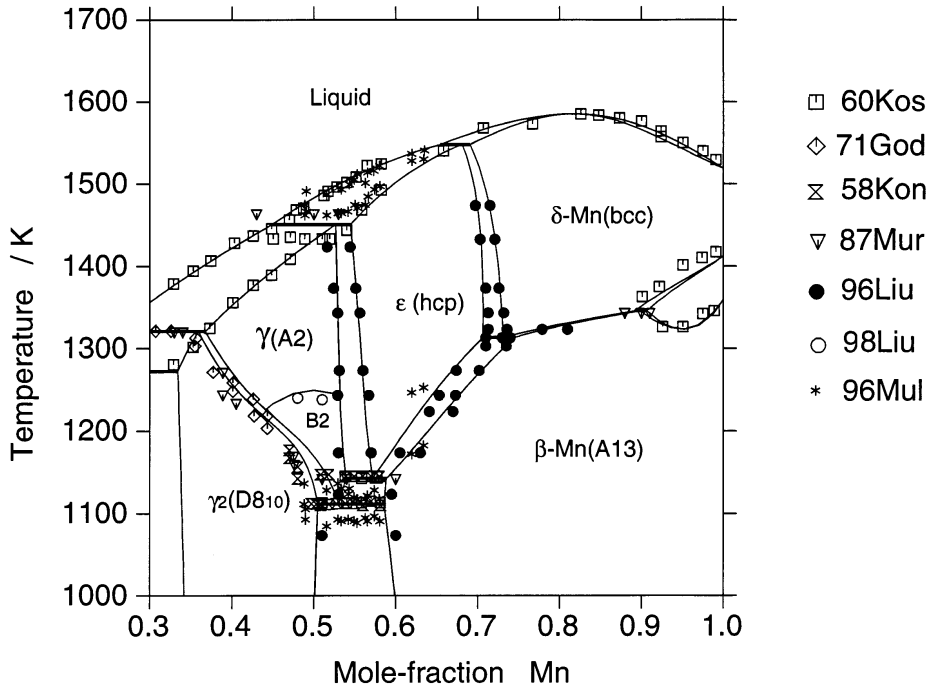

Fig. 7 Comparison of the calculated Mn-rich part of the Al-Mn phase diagram with experimental data

equilibrium determined by [96Liu]. The calculated temperatures pertaining to the ε/βMn phase equilibrium are somewhat higher than that experimentally determined by [96Liu].

It is also seen that the ε + βMn two-phase region becomes narrower with decreasing temperature. Calculations indicate that an underlying metastable minimum congruent point,

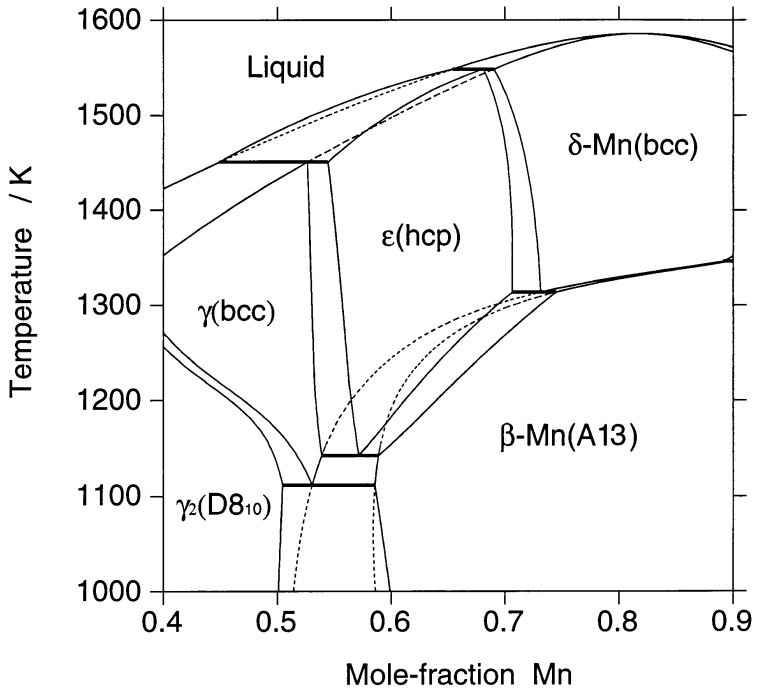

Fig. 8 Calculated metastable βMn/bcc and liquid/bcc phase equilibria

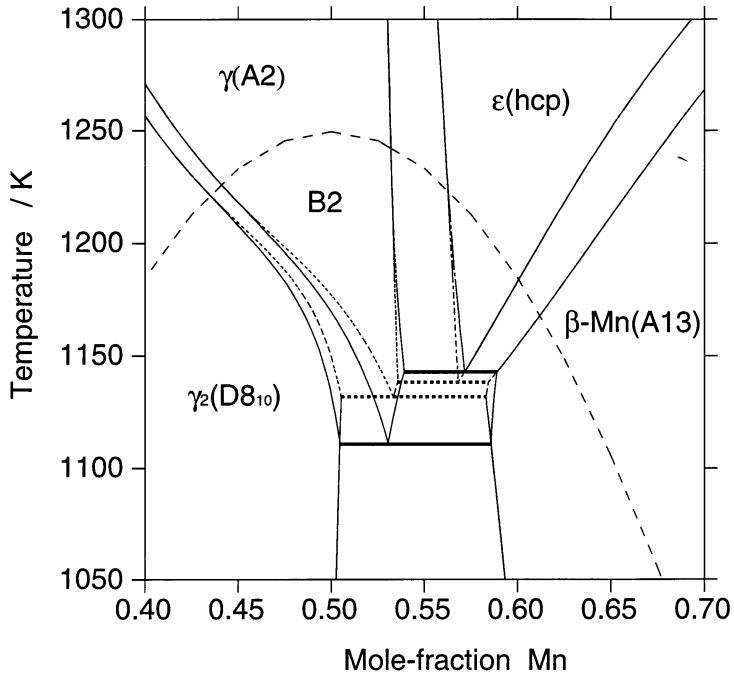

Fig. 9 Comparison of phase equilibria associated with the bcc phase in its disordered and ordered states. Ordered state is denoted by the solid line, disordered state by the short dashed line. Long dashed line indicates *A*2/*B*2 order-disorder transition.

Table 4 Comparison of enthalpies of formation assessed in the present calculation, [92Jan]'s assessment, and experimental data

Phase	This study	[92Jan]'s assessment	Measured value(a) from [60Kub], kJ/mol
Al_6Mn	–15.06	–15.00	–12.38
Al_4Mn	–21.23	–21.13	–21.67
$Al_{11}Mn_4$	–22.75	–23.65	–21.21
Al_8Mn_5(b)	–25.82	–23.74	–22.01, –20.71 at X_{Mn} = 0.5

(a) Estimated error, ±1.05. (b) The error of measurement for this compound may be larger, see text.

which is predicted to exist at about 1100 K and 50 at.% Mn, is the reason for this feature.

Calculated metastable βMn/bcc and liquid/bcc phase equilibria are shown in Fig. 8. The metastable βMn/bcc phase boundary shows a sharp curvature at about 65 at.% Mn. The effect of ordering in the bcc phase is illustrated in Fig. 9. The stability region for the γ phase becomes larger, and the temperatures of the eutectoid reactions $\varepsilon \leftrightarrow \gamma + \beta Mn$ and $\gamma \leftrightarrow \gamma_2 + \beta Mn$ become lower and higher, respectively, due to ordering. The highest temperature of *A*2/*B*2 order-disordered transition is at 1250 K, 50 at.% Mn.

6. Conclusions

A recalculation of the Al-Mn phase diagram has been carried out taking into account recent experimental data. The two-sublattice model has been applied to take into account the ordering reactions in the bcc phase. An agreement within 2 °C between calculated and experimentally determined invariant reaction temperatures has been obtained proving that the parameters determined in this study are better suited than the ones proposed in earlier studies to describe the phase diagram.

Acknowledgment

The authors would like to thank Dr. L. Chandrasekaran of DRA Farnborough, United Kingdom, for help in preparation of the manuscript for publication.

References

33Dix: E.H. Dix, W.L. Fink, and L.A. Willey, *Trans. AIME*, Vol 104, 1933, p 335-352
40Fah: E. Fahrenhorst and W. Hofmann, *Metallwirtschaft*, Vol 19, 1940, p 891-893 (in German)
43Phi: H.W.L. Phillips, *J. Inst. Met.*, Vol 69, 1943, p 275-316
45But: E. Butchers and W. Hume-Rothery, *J. Inst. Met.*, Vol 71, 1945, p 87-91
53Obi: I. Obinata, E. Hata, and K. Yamaji, *Jpn. J. Inst. Met.*, Vol 17, 1953, p 496-501
58Kon: H. Kono, *J. Phys. Soc. Jpn.*, Vol 13, 1958, p 1444
58Liv: V.A. Livanov and V.M. Vozdvizhenskii, *Tr. Mosk. Aviats. Tekhnol. Inst.*, Vol 31, 1958, p 84-99; cited in *Equilibrium Diagrams of Metallic Systems (1958)*, N.V. Ageev, Ed., Proizvod.-Izdatel., Moscow, 1961, p 6
60Koc: A.J.J. Koch, P. Hokkeling, M.G.v.d. Steeg, and K.J. DeVos, *J. Appl. Phys.*, Vol 13, 1960, p 75S-77S
60Kos: W. Koster and E. Wachtel, *Z. Metallkd.*, Vol 51, 1960, p 271-280 (in German)
60Kub: O. Kubaschewski and G. Meymer, *Trans. Faraday Soc.*, Vol 6, 1960, p 473-478
64Dri: M.H. Drits, E.S. Kadaner, E.M. Padezhnova, and N.R. Bochvar, *Russ. J. Inorganic Chem.*, Vol 9, 1964, p 759-762
69Sch: R.W. Schonorer and G.P. Mohanty, *Mater. Sci. Eng.*, Vol 4, 1969, p 243-245
70Hil: M. Hillert and L.I. Staffansson, *Acta Chem. Scand.*, Vol 24, 1970, p 3618-3626
71God: T. Godecke and W. Koster, *Z. Metallkd.*, Vol 62, 1971, p 727-732 (in German)
72Bat: G.I. Batalin, E.A. Belohorodov, B.A. Stuklao, and A.A. Tsheckowsky, *Ukr. Khim. Zh.*, Vol 38, 1972, p 825 (in Russian)
73Esi: Y.O. Esin, N.T. Bobrov, M.S. Pelrushevskii, and P.V. Geld, *Russ. J. Phys. Chem.*, Vol 47, 1973, p 1103-1105
76Ind: G. Inden, Project Meeting CALPHAD, V. Max Planck Inst. Eisenforsch., Düsseldorf, Germany, 1976, p 1-13
78Hil: M. Hillert and M. Jarl, *Calphad*, Vol 2, 1978, p 227-238
78Kau: L. Kaufman and H. Nesor, *Calphad*, Vol 2, 1978, p 325-340
83Nis: A.K. Nissen, F.R. de Boer, R. Boom, P.F. de Chatel, W.C.M. Mattens, and A.R. Miedema, *Calphad*, Vol 7, 1983, p 51-70
85Sun: B. Sundman, B. Jansson, and J.-O. Andersson, *Calphad*, Vol 9, 1985, p 153-190
87Mur: J.L. Murray, A.J. McAliter, R.J. Schaefer, L.A. Bendersky, F. Biancaniello, and D.L. Hoffat, *Metall. Trans.*, Vol 18A, 1987, p 385-392
90Mca: A.J. McAlster and J.L. Murray, *Binary Alloy Phase Diagrams*, 2nd ed., T.B. Massalski, P.R. Subramanian, H. Okamoto, and L. Kacprzak, Ed., ASM International, 1990, p 171-173
90Ell: M. Ellner, *Metall. Trans.* Vol 21A, 1990, p 1669
90Fer: A. Ferrandez Guillermet and W. Huang, *Int. J. Thermophys.*, Vol 11, 1990, p 949-969
91Din: A.T. Dinsdale, *Calphad*, Vol 15, 1991, p 317-425
92Jan: A. Jansson, *Metall. Trans.*, Vol 23A, 1992, p 2953-2962
94Oka1: H. Okamoto, *J. Phase Equilibria*, Vol 15, 1994, p 123-124
94Oka2: H. Okamoto and T.B. Massalski, *J. Phase Equilibria*, Vol 15, 1994, p 500-521
96Liu: X.J. Liu, R. Kainuma, H. Ohtani, and K. Ishida, *J. Alloy. Compd.*, Vol 235, 1996, p 256-261
96Mul: C. Muller, H.H. Stadelmaier, B. Reinsch, and G. Petzow, *Z. Metallkd.*, Vol 87, 1996, p 594-597
97Jan: A. Jansson, Ph.D. thesis, Royal Institute of Technology, Stockholm, Sweden, 1997
97Oka: H. Okamoto, *J. Phase Equilibria*, Vol 18 (No. 4), 1997, p 398-399
98Ish: K. Ishikawa, M. Ise, I. Ohnuma, R. Kainuma, and K. Ishida, *Ber. Bunsenges. Phys. Chem.*, Vol 102, 1998, p 1206-1210
98Kai1: R. Kainuma, M. Ise, K. Ishikawa, I. Ohnuma, and K. Ishida, *J. Alloy. Compd.*, Vol 269k, 1998, p 173-180
98Kai2: R. Kainuma, N. Sato, X.J. Liu, I. Ohnuma, and K. Ishida, *J. Alloy. Compd.*, Vol 266, 1998, p 191-200
98Liu: X.J. Liu, Ph.D. thesis, Tohoku University, Japan, 1998